J|A|C|S
ARTICLES
Published on Web 02/14/2004

A Q- and X-Band Pulsed Electron Nuclear Double Resonance Study of the Structure and Location of the Vanadyl Ions in the Cs Salt of Heteropolyacid $PVMo_{11}O_{40}$

Marlen Gutjahr,[†] Joachim Hoentsch,[†] Rolf Böttcher,[†] Oksana Storcheva,[‡] Klaus Köhler,*[,‡] and Andreas Pöppl*[,†]

Contribution from the Fakultät für Physik und Geowissenschaften, Universität Leipzig, Linnéstrasse 5, D-04103 Leipzig, Germany, and Anorganisch-chemisches Institut, Technische Universität München, Lichtenbergstrasse 4, D-85747 Garching, Germany

Received October 6, 2003; Revised Manuscript Received January 5, 2004; E-mail: poeppl@physik.uni-leipzig.de; klaus.koehler@ch.tum.de

Abstract: The location and coordination geometry of vanadium(IV) ions in the cesium salt of molybdovanadophosphoric heteropolyacid $Cs_4PVMo_{11}O_{40}$ were studied using orientation-selective pulsed ENDOR (electron nuclear double resonance) experiments. To enhance the orientation selectivity for the paramagnetic vanadyl species, these investigations were done at Q-band frequencies. It was possible to resolve interactions of the paramagnetic vanadyl ions (VO^{2+}) with all relevant nuclei, ^{1}H, ^{31}P, ^{51}V, and ^{133}Cs. The location of the vanadyl species was studied by determination of the complete ^{31}P hyperfine tensor. This approach was done for both the fresh and the calcined $Cs_4PVMo_{11}O_{40}$ materials, and no differences in the structures of the VO^{2+} complexes were found. The ENDOR results give experimental evidence for the location of the V(IV) ions. For both samples, it was possible to exclude the incorporation of V(IV) at the Mo sites. The VO^{2+} species are directly attached to the outer surface of the heteropolyanion and coordinated to four of the outer oxygen atoms with a V−P distance of 3.96 Å.

1. Introduction

Several heteropolyacids (HPA) and their salts are known as active heterogeneous catalysts for the selective oxidation of aldehydes and alkanes.[1,2] The catalytic performance of one specific HPA, $H_3PMo_{12}O_{40}$, can be enhanced by the substitution of V for Mo in the Keggin-type heteropolyanion.[3] Consequently, the location and the local coordination geometry of the incorporated vanadium ions are of special importance for the understanding of the catalytic activity of the HPA materials and for future development of tailor-made catalysts. Furthermore, this knowledge may also be helpful to understand and overcome the thus far poor thermal stability of the HPA-based catalyst, which is a major drawback for potential applications.[3]

Although vanadium originally incorporated into the HPA as V(V), it has been reported that a fractional amount of vanadium is always found as paramagnetic vanadyl ions[4,5] which can be characterized by electron spin resonance (ESR) spectroscopy. Due to the properties of the HPAs and their salts as oxidation catalysts and the specific role of vanadium in the reaction mechanism, a series of papers devoted to the characterization of V(IV) ions in HPAs by ESR have been published during the past decade.[5−7] Recently, Pöppl et al. succeeded in elucidating the V(IV) position in pure HPA materials, $H_4PVMo_{11}O_{40}$, by pulsed ENDOR experiments.[8] Likewise, some papers reported the structural and catalytic properties of heteropolymolybdate salts with different counterions, for example, iron,[9] cerium,[4] and cesium.[10−12] Despite various studies on the cesium salts of HPAs, the exact position of the vanadyl ions within the Keggin structure is still unknown. Until now, no conclusive experimental evidence has been given to substantiate the assumed substitution of V^{4+} ions for Mo inside the Keggin unit of the Cs salt ($Cs_4PVMo_{11}O_{40}$).[10]

The structure of the heteropolymolybdate salts is described on two levels. The main building block of the HPA, the so-called primary structure, contains the HPA anions which generally form the well-known structure of Keggin ions.[13,14]

[†] Universität Leipzig.
[‡] Technische Universität München.

(1) Lee, K.-Y.; Misono, M. In *Handbook of Heterogeneous Catalysis*; Ertl, G., Knözinger, H., Weitkamp, J., Eds.; VCH: Weinheim, 1997; Vol. 1, p 118.
(2) Kozhevnikov, I. V. *Catal. Rev.-Sci. Eng.* **1995**, *37*, 311.
(3) Mizuno, N.; Misono, M. *J. Mol. Catal.* **1994**, *86*, 319 and literature cited therein.
(4) Aboukaïs, A.; Haubtmann, C.; André, J. J.; Desquilles, C.; Dourdin, M.; Mathes-Juventin-Andrieu, I.; Aïssi, F. C.; Guelton, M. *J. Chem. Soc., Faraday Trans.* **1995**, *91*, 1025.
(5) Fricke, R.; Jerschewitz, H.-G.; Öhlmann, G. *J. Chem. Soc., Faraday Trans. 1* **1986**, *82*, 3479.
(6) Bayer, R.; Marchal, C.; Liu, F. X.; Tézé, A.; Hervé, G. *J. Mol. Catal. A: Chem.* **1996**, *110*, 65.
(7) Inumaro, K.; Ono, A.; Kubo, H.; Misono, M. *J. Chem. Soc., Faraday Trans. 1* **1998**, *94*, 1765.
(8) Pöppl, A.; Manikandan, P.; Köhler, K.; Maas, P.; Strauch, P.; Böttcher, R.; Goldfarb, D. *J. Am. Chem. Soc.* **2001**, *123*, 4577.
(9) Langpage, M.; Millet, J.-M. M. *Appl. Catal., A: General* **2000**, *200*, 89.
(10) Lee, J. K.; Russo, V.; Melsheimer, J.; Köhler, K.; Schlögl, R. *Phys. Chem. Chem. Phys.* **2000**, *2*, 2977.
(11) Berndt, S.; Herein, D.; Zemlin, F.; Beckmann, E.; Weinberg, G.; Schütze, J.; Mestl, G.; Schlögl, R. *Ber. Bunsen-Ges. Phys. Chem.* **1998**, *102*, 763.
(12) Mestl, G.; Ilkenhans, T:; Spielbauer, D.; Dieterle, M.; Timpe, O.; Kröhnert, J.; Jentoft, F.; Knözinger, H.; Schlögl, R. *Appl. Catal., A: General* **2001**, *210*, 13.
(13) Keggin, J. F. *Proc. R. Soc.* **1934**, *A144*, 75.
(14) D'Amour, H.; Allmann, R. *Z. Kristallogr.* **1976**, *143*, 1.

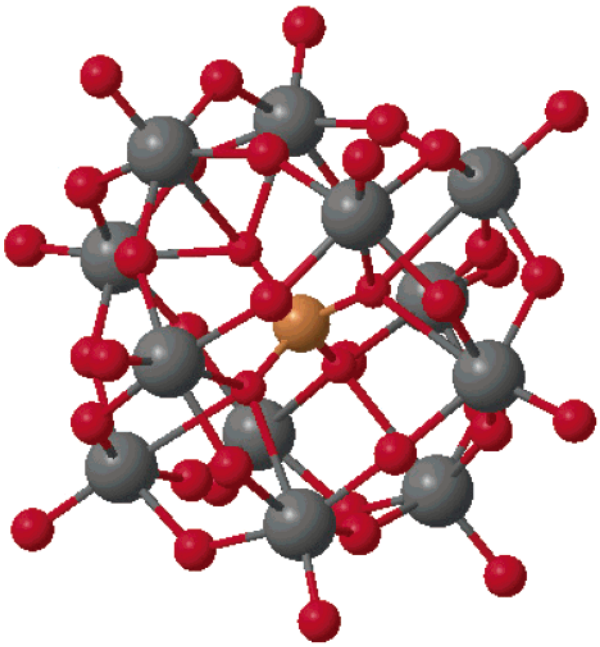

Figure 1. Structure of the Keggin-type $[PVMo_{11}O_{40}]^{4-}$ heteropolyanion.

This is schematically shown in Figure 1. In this example, the Keggin unit consists of a central phosphorus atom surrounded by 12 oxygen octahedrons which contain molybdenum atoms. Four types of oxygen atoms can be distinguished. First, four central oxygens O(1) form a PO_4 tetrahedron with the central P. Two kinds of bridging oxygen atoms O(2) and O(3) then connect the Mo octahedrons. Finally, 12 terminal oxygen atoms O(4) form double bonds to the neighbored transition metal ions. The arrangement of this primary structure together with counterions and water molecules forms the secondary structure. Concerning the secondary structure of heteropoly compounds with Cs^+ as counterions, several papers were recently published.[11,12,15,16] It has been reported that the presence of Cs leads to a stabilization of heteropoly compounds.[12] Berndt et al. described the secondary structure of several Cs heteropoly salts as a cubic structure with variable site occupations.[11] The structure of the cesium salt of the vanadium-trisubstituted dodecatungstophosphate anion was determined by X-ray analysis.[16] Furthermore, the lack of mobility of larger cations such as Cs^+ as compared to, for example, Li^+ or Na^+ has been explained by the possible coordination of the Cs ions to more oxygen atoms.[15] The exact position of the Cs^+ cations with respect to the Keggin anions is, to our knowledge, still not known for $Cs_4PVMo_{11}O_{40}$ heteropoly compounds. Another motivation for this study was to use information about the location of the vanadyl ions to gain insight into the coordination geometry of the Cs counterions by studying the Cs hyperfine (hf) interaction. However, these studies are currently underway and are not part of the present investigation.

Various ESR studies of the paramagnetic vanadyl species in several HPA materials showed that the principal values of the electron Zeeman interaction tensor **g** and the ^{51}V hf coupling tensor $\mathbf{A}^V$ are sensitive to the modifications of the V(IV) local environment.[5−8] The amount of paramagnetic V(IV) species in the fully exchanged Cs salt, $Cs_4PVMo_{11}O_{40}$, is estimated to be about 0.5 mol % of the total vanadium content for the untreated material, and about 0.2 mol % after thermal treatment at 573 K. This is significantly lower than in the corresponding acid, $H_4PVMo_{11}O_{40}$.[10] Also, it has been reported, again in contrast to the acid, that the ESR signal of the $Cs_4PVMo_{11}O_{40}$ material displays no significant changes after thermal treatment of up to 773 K. This simplifies the situation in comparison to the very complex pure acid, $H_4PVMo_{11}O_{40}$. Therefore, the Cs_4 salt obtains some model character. However, the **g** and $\mathbf{A}^V$ tensors are not sensitive to the second and higher coordination spheres of vanadium(IV), and the coordination geometry and position of the paramagnetic vanadium ions cannot be deduced from ESR spectroscopic results.

To overcome the limitations of the continuous wave ESR technique, the pulsed electron nuclear double resonance (ENDOR) spectroscopy was applied at X- and Q-band frequencies. By using the high-resolution methods, it was possible to resolve the hf interaction tensor of the unpaired electron on the V(IV) ion with the phosphorus nucleus at the central position of the Keggin ion. The ^{31}P hf coupling tensor gives the P−V(IV) distance which reveals information about the location of the vanadyl ions as the central position of P is assured. In this way, the ENDOR approach turned out to be a powerful tool for the determination of the local environment of the paramagnetic V(IV) ions within the Cs salts of the HPAs.

2. Experimental Section

Sample Preparation. $H_4PVMo_{11}O_{40}$ was prepared by dissolving stoichometric quantities of V_2O_5 (1.25 mmol) and MoO_3 (27.5 mmol) in the appropriate amounts of phosphoric acid. H_3PO_4 was added dropwise for 1 h, and the resulting mixture was refluxed for 4 h. Evaporation of water from the clear red-brown solution resulted in a red-brown precipitate.

A 116 mM aqueous solution of Cs_2CO_3 was added dropwise to a 14 mM solution of boiling $H_4PVMo_{11}O_{40}$. After the addition was complete, a yellow precipitate formed. Thermally treated samples were obtained by thermal treatment of the fresh $Cs_4PVMo_{11}O_{40}$ at 573 K in O_2(35%)/Ar or air/Ar streams. Several experiments were undertaken under reducing atmosphere (methanol stream, 0.2% CH_3OH in Ar). All samples were investigated by ESR as well as ENDOR spectroscopy; qualitatively the same results (concerning structural conclusions) were obtained for all thermal treatments until 573 K. After the treatment, the samples were immediately transferred to ESR quartz glass tubes and sealed without contact to air. The fresh and thermally treated $Cs_4PVMo_{11}O_{40}$ samples are denoted as PVMoCs-1 and PVMoCs-2, respectively.

Spectroscopic Measurements. Two-pulse field-swept electron spin−echo and pulsed ENDOR experiments were performed at X-band frequencies (9.7 GHz) with a Bruker ESP 380 spectrometer and at Q-band frequencies (35 GHz) with a spectrometer with a home-built microwave (mw) pulse unit and a commercial magnet system from a BRUKER EMX cw Q-band instrument. The measurements were carried out at 6 K. For the two-pulse field-swept ESE experiments, mw pulse lengths of $t_{\pi/2} = 16$ ns for $\pi/2$ pulses and $t_\pi = 32$ ns for π pulses with a pulse delay of $\tau = 120$ ns were used at X-band, and $t_{\pi/2} = 90$ ns for $\pi/2$ pulses and $t_\pi = 120$ ns for π pulses with a pulse delay of $\tau = 400$ ns were used at Q-band. The Mims ENDOR pulse sequence for X-band frequencies was applied with $t_{\pi/2} = 96$ ns and a pulse delay between the first two $\pi/2$ pulses ($\tau = 1000$ ns) for X-band experiments. The radio frequency (rf) pulse width was $t_{rf} = 10\ \mu$s. Q-band Mims ENDOR experiments were run with $t_{\pi/2} = 90$ ns, $t_{rf} = 25\ \mu$s, and $\tau = 300$ ns.

(15) Tsujimichi, K.; Kubo, M.; Vetrivel, R.; Miyamoto, A. *J. Catal.* **1995**, *157*, 569.
(16) Kawafune, I.; Tamura, H.; Matsubayashi, G. *Bull. Chem. Soc. Jpn.* **1997**, *70*, 2455.

3. Simulation of Orientation-Selective ENDOR Spectra

Because several papers discussing the theory of the orientation-selective pulsed ENDOR technique have been published,[17−19] we will only very briefly describe the simulation procedure used. First, the **g** tensor orientations contributing to the ESR resonance fields at the magnetic field position that was selected for the performance of the orientation-selective ENDOR experiment had to be determined. The **g** tensor orientations are defined by pairs (Θ_i, Φ_i) of horizontal and azimuthal angles Θ and Φ. The dominating interactions in the ESR spectrum of the vanadyl ions are the electron Zeeman and the vanadium hf interactions with the coaxial tensors **g** and $\mathbf{A}^{\mathrm{V}}$. The ESR resonance position at the selected magnetic field B_0 is given by

$$B_0 = \frac{h\nu_{\mathrm{mw}} - \sum_i A(\Theta,\Phi) m_i^{\mathrm{V}}}{\beta_e g(\Theta,\Phi)} \quad (1)$$

with the mw frequency ν_{mw} and the magnetic spin quantum numbers of the ^{51}V nuclei $m_i^{\mathrm{V}} = -^7/_2, -^5/_2, ..., ^7/_2$. The effective g and hf coupling A are given by

$$g(\Theta,\Phi) = \left(\sum_j g_{jj}^2 l_j^2\right) \quad (2)$$

and

$$A(\Theta,\Phi) = \left(\frac{\sum_j (A_{jj}^{\mathrm{V}} g_j l_j)^2}{g(\Theta,\Phi)^2}\right)^{1/2} \quad (3)$$

with the direction cosines $l_x = \cos\Phi \sin\Theta$, $l_y = \sin\Phi \cos\Theta$, $l_z = \cos\Theta$ defining the orientation of the external magnetic field $\mathbf{B}_0$ with respect to the **g** tensor frame. The orientations (Φ_i, Θ_i) corresponding to the observer field B_0 are determined by calculating the ESR spectrum according to eqs 1−3. Under the assumption that the bandwidth of the mw pulses is smaller than the inhomogeneous ESR line width $\Delta B_{1/2}^{\mathrm{inh}}$, all of the **g** tensor orientations which lead to a resonance position within the interval $B_0 \pm \Delta B_{1/2}^{\mathrm{inh}}$ are collected.

Subsequently, the ENDOR spectrum is calculated from the selected orientations by an exact diagonalization of the spin Hamiltonian given in the **g** tensor principal axes system

$$\hat{\mathbf{H}} = \beta_e B_0(0,0,1)\tilde{\mathbf{R}}(\Phi_i,\Theta_i,0)\mathbf{g}\hat{\mathbf{S}} - \beta_n g_n B_0(0,0,1)\tilde{\mathbf{R}}(\Phi_i,\Theta_i,0)\hat{\mathbf{I}}^{\mathrm{P}} + \hat{\mathbf{S}}\tilde{\mathbf{R}}(\alpha,\beta,\gamma)\mathbf{A}^{\mathrm{P}}\mathbf{R}(\alpha,\beta,\gamma)\hat{\mathbf{I}}^{\mathrm{P}} \quad (4)$$

with g_n being the nuclear g factor and β_e, β_n, **S**, and **I** having their usual meanings. The first two addends in eq 4 are due to the electron and the nuclear Zeeman interactions, respectively. The third term defines the shf interaction of the unpaired electron with the nuclear spin of the phosphorus ligands, where $\mathbf{A}^{\mathrm{P}}$ is the ligand shf interaction tensor. **R** is the Euler matrix, where (α,β,γ) denote a set of Euler angles which define the transformation of the diagonal $\mathbf{A}^{\mathrm{P}}$ tensor into the **g** tensor coordinate frame. From the differences of the obtained eigenvalues E, the ENDOR transition frequencies $\nu_{ij} = (E_i - E_j)/h$ between the eigenvalues E_i and E_j within the two electron spin manifolds $m_S = \pm^1/_2$ are obtained. For each transition frequency, the relative ENDOR intensity P_{ij} is calculated from the matrix elements

$$P_{ij} = \langle\psi_i|B_{\mathrm{rf}}(0,1,0)\tilde{\mathbf{R}}(\Phi_i,\Theta_i,0)(-\beta_n g_n \hat{\mathbf{I}}^n + \beta_e \mathbf{g}\hat{\mathbf{S}})|\psi_j\rangle^2 \quad (5)$$

where ψ_i and ψ_j are the eigenvectors belonging to the spin states i and j. Here, the hyperfine enhancement means the interaction between the electron spin and the radio frequency field B_{rf} was taken into account. To simulate the orientation-selective ENDOR spectra, the described procedure was repeated for each set of contributing **g** tensor orientations. Finally, the ENDOR spectrum is obtained by summing all of the individual ENDOR spectra using a Gaussian weighting function with a variance $\Delta B_{1/2}^{\mathrm{inh}}$.

4. Results

Field-Swept ESE. Two-pulse field-swept ESE spectra of $Cs_4PVMo_{11}O_{40}$ before and after thermal treatment were taken at X- and Q-band frequencies at 7 K. Figure 2a illustrates the X-band echo-detected ESR spectrum of the fresh cesium salt sample (PVMoCs-1) in comparison with the sample thermally treated at 573 K (PVMoCs-2). In Figure 2b, the Q-band field-swept ESE spectra of both samples are shown. There is not much difference between the experimental spectra of these two samples in either the X- or the Q-band experiment. Both powder spectra can be described by an axially symmetric **g** tensor of the V(IV) ion ($S = ^1/_2$, $3d^1$). Due to the hf interaction of the unpaired electron spin with the vanadium nucleus (nuclear spin $I = ^7/_2$), a splitting of the spectrum into eight lines is observed. The spin-Hamiltonian parameters were determined by simulating the experimental ESR powder patterns using second-order perturbation theory. The simulations of all of the experimental echo-detected ESR spectra could be done with the same set of spin-Hamiltonian parameters: $g_{\|} = 1.936$, $g_{\perp} = 1.973$ (with an estimated error of ± 0.002), and an axially symmetric ^{51}V hf coupling tensor $\mathbf{A}^{\mathrm{V}}$ with principal values $A_{\|}^{\mathrm{V}} = 0.0147$ cm^{-1} and $A_{\perp}^{\mathrm{V}} = 0.0050$ cm^{-1} (each with an estimated error of ± 0.0002 cm^{-1}). The only difference between the fresh sample spectra and the thermally treated ones is the line width $\Delta B_{1/2}$. In the case of the thermally treated sample, the line width is slightly larger. At the X-band frequency, $\Delta B_{1/2}$ is 2.4 mT for PVMoCs-1 and 2.6 mT for PVMoCs-2. The same tendency toward line broadening was also obtained at Q-band frequencies, where $\Delta B_{1/2}$ (PVMoCs-1) = 2.4 mT and $\Delta B_{1/2}$ (PVMoCs-2) = 2.9 mT. The simulated spectra shown in Figure 2a and 2b were calculated in each case using $\Delta B_{1/2} = 2.4$ mT. The slightly larger line widths observed for PVMoCs-2 are probably due to an increase of g and A strain effects upon thermal treatment of the $Cs_4PVMo_{11}O_{40}$ material.

Additionally, ESR spectra were taken at 300 K (not shown), and the corresponding spin-Hamiltonian parameters were determined: $g_{\|}^{\mathrm{RT}} = 1.937$, $g_{\perp}^{\mathrm{RT}} = 1.976$, $A_{\|}^{\mathrm{V}}(\mathrm{RT}) = 0.0147$ cm^{-1}, and $A_{\perp}^{\mathrm{V}}(\mathrm{RT}) = 0.005$ cm^{-1}. They coincide almost exactly with the experimental findings at 8 K.

Although it is well known that the ESR spectra of the pure heteropoly acid, $H_4PVMo_{11}O_{40}$, drastically change after thermal treatment, no difference in the spin-Hamiltonian parameters before and after thermal treatment was found for $Cs_4PVMo_{11}O_{40}$, in concordance with the literature.[10] The reported ESR param-

(17) Hoffmann, B. M.; Martinsen, J.; Venters, R. A. *J. Magn. Reson.* **1984**, *59*, 110.
(18) Hurst, G. C.; Henserson, T. A.; Kreilick, R. W. *J. Am. Chem. Soc.* **1985**, *107*, 7294.
(19) Kreiter, A.; Hüttermann, J. *J. Magn. Reson.* **1991**, *93*, 12.

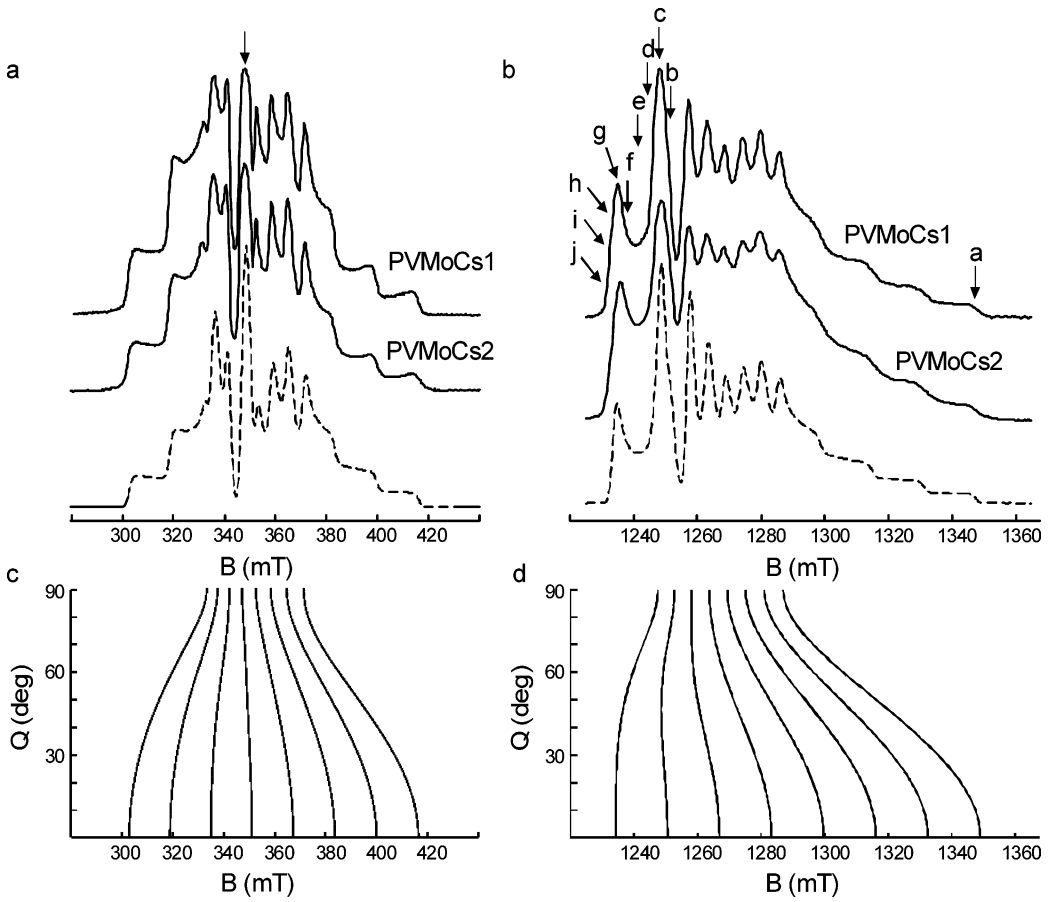

Figure 2. Two-pulse field-swept ESE spectra recorded at 7 K for V(IV) ions in fresh (PVMoCs-1) and thermally treated (T = 573 K, PVMoCs-2) $Cs_4PVMo_{11}O_{40}$ samples: experimental (solid lines) and simulated (dashed lines) (a) X-band and (b) Q-band spectra. The arrows indicate the field positions for the pulsed ENDOR experiments. Calculated magnetic resonance fields dependent on the angle Θ between the $g_{||}$ axis of the V(IV) **g** tensor and the external magnetic field at (c) X-band and (b) Q-band frequencies.

eters for the fully exchanged Cs salt are in good agreement with our results. Within the scope of that ESR study of V^{4+} in heteropoly compounds, the ESR signal of $Cs_4PVMo_{11}O_{40}$ was assigned to V^{4+} ions substituted for Mo in the Keggin unit.[10]

To select proper field positions for the orientation-selective ENDOR measurements, the ESR resonance fields were calculated as a function of the angle Θ between the $g_{||}$ axis of the V(IV) **g** tensor and the external magnetic field. These calculations were made by determining the principal values of the **g** and the $\mathbf{A}^V$ tensors. The resulting plots for X- and Q-band experiments are presented in Figure 2c and 2d, respectively.

Pulsed ENDOR. X-band pulsed ENDOR experiments of the fresh and thermally treated Cs_4 salts revealed almost identical spectral features. The overview X-band Mims ENDOR spectra for both samples were recorded at the so-called powder position of the V(IV) ESR spectrum and are displayed in Figure 3. The spectra show four groups of signals each centered at 1.94, 3.88, 5.98, and 14.78 MHz. These ENDOR signals are assigned to superhyperfine (shf) interactions between the paramagnetic V(IV) centers and the ^{133}Cs, ^{51}V, ^{31}P, and ^{1}H nuclei, respectively, resting on the appropriate nuclear Larmor frequencies ν_{Cs} = 1.938 MHz, ν_V = 3.884 MHz, ν_P = 5.982 MHz, and ν_H = 14.778 MHz for B = 347.1 mT. The broad ^{133}Cs signal was distorted by blind spots appearing at ν_{Cs} and $\nu_{Cs} \pm 0.5$ MHz and was caused by the τ-dependent suppression effect in the Mims ENDOR experiment.[20] It should be mentioned that the ^{51}V ENDOR signal does not belong to the V(IV) species whose hf interaction has already been resolved in the ESR pattern, but is due to the weak shf interactions between V(IV) and more distant diamagnetic V(V) nuclei. Both spectra show one intense proton ENDOR signal from distant protons at ν_H whose outer wings are also affected by blind spots. The phosphorus ENDOR signal gives a line at the ^{31}P Larmor frequency ν_P for both the fresh and the thermally treated materials. The line is due to distant ^{31}P nuclei. Additionally, in both cases, a doublet symmetric to ν_P appears with a splitting of about 0.36 MHz.

Because the central position of the phosphorus atom in the Keggin unit is well known from crystallographic data, it is a promising approach to ascertain the location of the V(IV) ions by using the dipolar shf interactions of the ^{31}P nuclei. To determine both the principal values of the ^{31}P shf coupling tensor $\mathbf{A}^P$ and its orientation with respect to the **g** tensor frame of the V(IV) ions, orientation-selective pulsed ENDOR experiments were performed. For these purposes, the magnetic resonance fields depending on the angle Θ were calculated for X-band as well as for Q-band frequencies (Figure 2c and 2d). On the basis of those results, the advantage of taking measurements at frequencies higher than the X-band is evident for many systems. Changing to Q-band frequencies means significantly enhancing the separation of the $g_\perp$ from the $g_{||}$ region. Performing the orientation-selective pulsed ENDOR experiments at Q-band frequencies is a special advantage for vanadium. The represen-

(20) Gemperle, C.; Schweiger, A. *Chem. Rev.* **1991**, *91*, 1481.

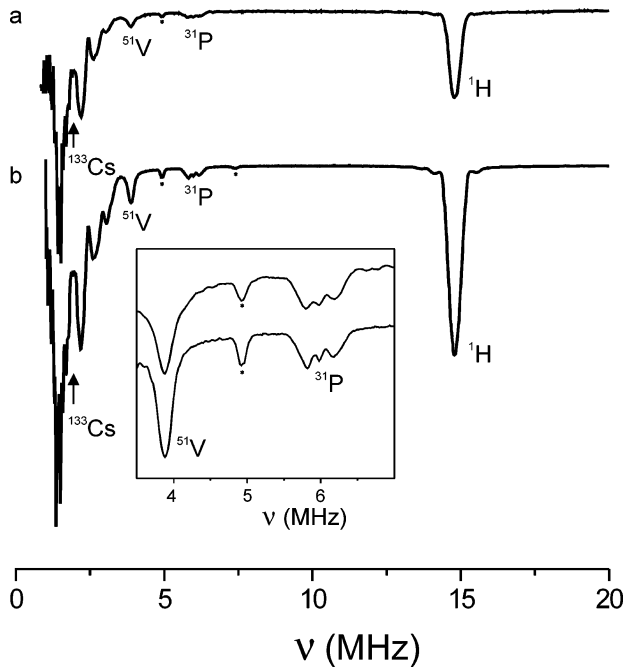

Figure 3. X-band Mims ENDOR spectra at 5 K of (a) fresh and (b) thermally treated ($T = 573$ K) $Cs_4PVMo_{11}O_{40}$ materials recorded at $B =$ 347.1 mT (indicated by an arrow in Figure 2a). The signals marked by asterisks are artifacts due to proton harmonics.

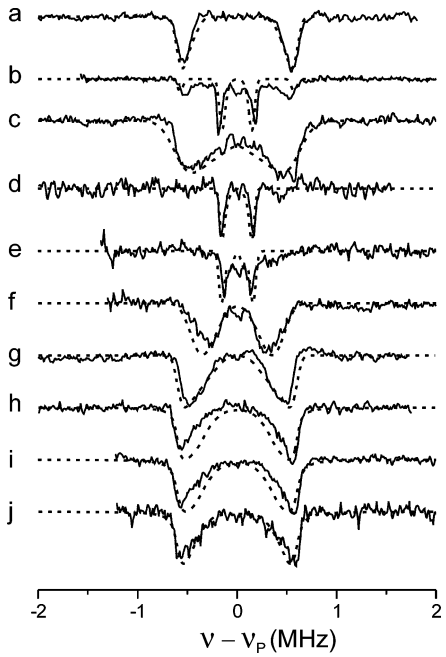

Figure 4. Experimental (solid lines) and simulated (dashed lines) orientation-selective ^{31}P Mims ENDOR Q-band spectra of V(VI) species in fresh $Cs_4PVMo_{11}O_{40}$ materials (PVMoCs-1). The appropriate field positions are indicated in Figure 2.

tation of the ESR resonance fields as a function of the angle Θ (Figure 2c and 2d) clarifies that, only at Q-band, but not at X-band frequencies, the low field V hf transition, corresponding to the nuclear quantum number $m_I = +^7/_2$, is separate from other hf transitions. Because the $g_{||}$ region of the $m_I = +^7/_2$ hf transition covers a broad range of angles in the ESR powder pattern ($0 \le \Theta \le 30°$), it was advantageous to also perform the orientation-selective ENDOR experiment for the $g_{||}$ orientation at the high-field edge of the field-swept ESE spectrum. Here, the orientation selection is even better because the $m_I = -^7/_2$ high field V hf transition displays a stronger dependency on the angle Θ than does the $m_I = +^7/_2$ transition.

The orientation-selective Q-band Mims ENDOR spectra of the fresh $Cs_4PVMo_{11}O_{40}$ are shown in Figure 4. The field positions where the ENDOR measurements were done are indicated by arrows in Figure 2b. In each case, these data represent a pair of ENDOR signals symmetric to the ^{31}P Larmor frequency ν_P. Thus, they are assigned to ^{31}P nuclear transitions of a single phosphorus nucleus close to the paramagnetic V(IV) center. The ENDOR signals arise from transitions belonging to the two different electron spin manifolds ($m_S = \pm^1/_2$) within the limits of the weak coupling case ($A^P < 2\nu_P$). Corresponding to the calculated ESR resonance fields, two spectra taken at the $g_{||}$ edge of the two-pulse field-swept ESE spectrum, with tensor orientations Θ close to zero, were selected and are displayed in Figure 4a and 4j. At these spectral positions, a maximum splitting of about 1.2 MHz is observed. The minimum splitting of about 0.3 MHz is detected at the $g_\perp$ position ($\Theta =$ 90°). The ENDOR spectra suggest an axially symmetric ^{31}P shf tensor almost coaxial to the V(IV) electron **g** tensor. Simulations of the orientation-selective Mims ENDOR spectra give a ^{31}P shf coupling tensor $\mathbf{A}^P$ with axial symmetry. The principal values of $\mathbf{A}^P$ are $A_\perp{}^P = -0.32$ MHz and $A_{||}{}^P = 1.2$ MHz. By simulating the spectra, it was possible to ensure the different signs of the phosphorus hf principal values. Especially the region with orientations from about 60° to 90° between the $g_{||}$ principal axis and the external magnetic field shows a large deviation from the experimental data for $A_\perp{}^P$ and $A_{||}{}^P$ with the same sign. Furthermore, simulations showed that the $A_{||}{}^P$ axis is pointing approximately in the $g_{||}$ direction of the electron **g** tensor of the vanadyl ions. The best concordance with the experimental spectra could be achieved with the angle $\beta = 12°$ between the $g_{||}$ and the $A_{||}{}^P$ axis. In particular, the ENDOR line shape of the spectra (Figure 4h, i, and j), where only the orientations with $\Theta < 45°$ contribute to the orientation-selective ENDOR experiments, coincides better with the spectral simulations for a nonzero angle $\beta = 12°$. The estimated error for the angle β is about $\pm 3°$. In contrast to earlier pulsed ENDOR results concerning the location of V(IV) in dehydrated HPA,[8] no experimental evidence for the existence of more than one P shf tensor could be found.

The simulations of the experimental ENDOR data took into account the τ-dependent suppression effect in the Mims ENDOR experiment.[20] In accordance with the experimental pulse delay $\tau = 300$ ns, blind spots will occur at $\nu = \nu_P$ and $\nu = \nu_P \pm 1.6$ MHz, whereas the maximum intensity in the ENDOR spectra is expected at $\nu_P \pm 0.85$ MHz. The outer blind spots at $\nu_P \pm$ 1.6 MHz do not affect the ENDOR pattern at all. However, the central blind spot leads to a strong decrease in the signal intensity in the region close to the ^{31}P Larmor frequency.

Mims ENDOR experiments were performed on the thermally treated $Cs_4PVMo_{11}O_{40}$ material for the field positions expected to influence the ^{31}P hf parameter noticeably. In Figure 5, selected experimental spectra of PVMoCs-2 are shown in comparison with the ENDOR spectra of PVMoCs-1. The Mims ENDOR spectra of both the fresh and the thermally treated materials display no significant differences, indicating an identical ^{31}P hf coupling tensor for the fresh and the treated $Cs_4PVMo_{11}O_{40}$ sample and the same orientation of $\mathbf{A}^P$ with respect to the **g** tensor frame.

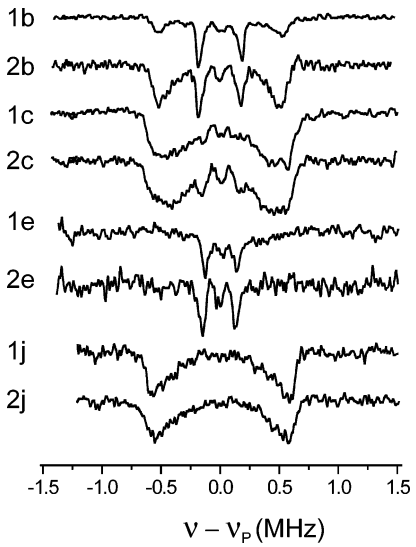

Figure 5. Comparison between Mims ENDOR Q-band spectra at selected field positions (positions b, c, e, and j in Figure 2b) from fresh PVMoCs-1 (1b, 1c, 1e, 1j) and thermally treated PVMoCs-2 (2b, 2c, 2e, 2j) $Cs_4PVMo_{11}O_{40}$ materials.

5. Discussion

The obtained ESR spin-Hamiltonian parameters for the fresh and the thermally treated $Cs_4PVMo_{11}O_{40}$ are typical for paramagnetic vanadium existing as vanadyl (VO^{2+}) species with the unpaired electron located in the $3d_{xy}$ orbital.[21] The parameters are in good agreement with the recently reported ESR results of the fully exchanged Cs salt of the heteropolyacid $PVMo_{11}O_{40}$.[10] Comparing the ^{51}V hf interaction parameters of the vanadyl ions in the fresh and the treated $H_4PVMo_{11}O_{40}$ materials[8] with those of the Cs_4 salt of the HPA, one can observe that $A_{||}^{P}$ (PVMoCs-1) is roughly the same for the dehydrated, pure HPA material, but differs for the fresh, pure HPA. It has been reported that in the fresh HPA material the vanadyl ions are coordinated to crystallization water molecules, resulting in vanadyl pentaaqua complexes.[6,8] After dehydration of the $H_4PVMo_{11}O_{40}$ material, the VO^{2+} ions were determined to be attached to the outer surface of the heteropolyanions and to coordinate to the bridging oxygens O(2) and O(3).[8] Thus, for the pure HPA materials, a strong change in the coordination geometry of the vanadyl ions was found after thermal treatment, as has already been shown by different ESR parameters.

On the contrary, we found no significant differences in the principal values of both the electron **g** tensor of the vanadyl ions and the ^{51}V hf coupling tensor $\mathbf{A}^{V}$ for the $Cs_4PVMo_{11}O_{40}$ material both before and after thermal treatment. According to these results, it could be implied that the location and the coordination geometry of the incorporated V(IV) do not significantly change when the sample is heated. To elucidate the exact position and the coordination geometry of the V(IV) ions, pulsed ENDOR experiments were performed. Of great significance for this study was the ability to run the ENDOR experiments at Q-band frequencies because their orientation selectivity is considerably enhanced in comparison to conventional X-band experiments.

The X-band ^{1}H ENDOR signals (Figure 3) are evidence that there are no strongly coupled protons in both the fresh and the thermally treated samples (also not due to adsorbed methanol from reduction trials, see Experimental Section). The obtained ^{1}H ENDOR signal at ν_H is due to the weak interaction with distant protons.

From the determined ^{31}P hf coupling tensor, the location of the vanadyl ions can be deduced. Because there is no doubt about the central position of the phosphorus nucleus within the Keggin unit, the V(IV) position can be ascertained from the dipolar ^{31}P hf coupling tensor $\mathbf{T}^{P}$ and its orientation with respect to the **g** tensor frame. From the principal values of the phosphorus shf tensor for PVMoCs-1, $A_{\perp}^{P} = -0.32$ MHz and $A_{||}^{P} = 1.20$ MHz, we determine an isotropic phosphorus shf coupling of $A_{iso}^{P} = 0.18$ MHz. This translates to unpaired electron spin density in the 3s orbital of P ($\rho_{3s}^{P} = 1.4 \times 10^{-3}$%). Furthermore, we can deduce the principal values $T_{\perp}^{P} = -0.51$ MHz and $T_{||}^{P} = 1.02$ MHz of $\mathbf{T}^{P}$ with an error of about $\Delta T_{\perp}^{P} = \pm 0.01$ MHz. With those results, the distance between the phosphorus atom and the vanadyl ion was estimated by using the point dipole approximation to be $r_{V-P} = (3.96 \pm 0.03)$ Å. The use of the point dipole approximation is justified because of the very small value for ρ_{3s}^{P}, indicating the spread of wave function of the unpaired electron over HPA is negligible.

The experimental results did not indicate the existence of more than one vanadium species. Different coordination structures of the VO^{2+} ions would cause different phosphorus shf coupling tensors and, hence, should be observable in the ^{31}P Mims ENDOR spectra. For instance, in the case of the pure HPA material, $H_4PVMo_{11}O_{40}$, three different vanadyl species were determined. They showed up in the pulsed ENDOR spectra as pronounced shoulders on the high- and low-frequency wings of the phosphorus ENDOR signals symmetrical to the ^{31}P Larmor frequency.[8]

The vanadium ions in the fully exchanged Cs salt of HPA (Cs_4HPA) are not expected to move to a bridge-site position between the heteropolyanions because the bulky Cs ions and the rigid lattice would hinder this. For that reason, it was assumed by Lee et al. that the V^{4+} ions could be substituted for the Mo^{6+} ions in the Keggin unit.[10]

The distance between the central phosphorus atom and the Mo sites in the $[PMo_{12}O_{40}]^{3-}$ anion was determined to be 3.55 Å.[14] Likewise, an X-ray analysis of A-β-$Cs_{5.4}H_{0.6}[PV_3W_9O_{40}]\cdot 12H_2O$ found P−V and P−W distances to be within the range from 3.54 to 3.56 Å for V and W located at the known metal position in the Keggin unit.[16] For that reason, the incorporation of the paramagnetic V(IV) ion at the molybdenum sites can be excluded for $Cs_4PVMo_{11}O_{40}$ on the basis of the presented ENDOR results.

The $g_{||}$ axis of the vanadyl ions is defined as the direction of the V=O double bond of the VO^{2+} species. Because the angle $\beta = 12°$ between the $g_{||}$ and the $A_{||}$ principal axes has been determined, a small tilt angle of about 12° between the vector joining the vanadium and the phosphorus atom (R_{V-P}) and the V=O bond direction must exist.

On the basis of the orientation-selective pulsed ENDOR results, we conclude that the VO^{2+} ions are attached to the outer surface of the heteropolyanion. We propose a four-fold coordination for the V^{4+} ions to the bridging oxygens O(2) and O(3). Taking this into consideration, the most probable complex structure for the VO^{2+} complexes in both the fresh and the thermally treated $Cs_4PVMo_{11}O_{40}$ materials is a slightly distorted

(21) Catana, G.; Ramachandra Rao, R.; Wechhuysen, B. M.; Van Der Voort, P.; Vansant, E.; Schoonheydt, R. A. *J. Phys. Chem. B* **1998**, *102*, 8005.

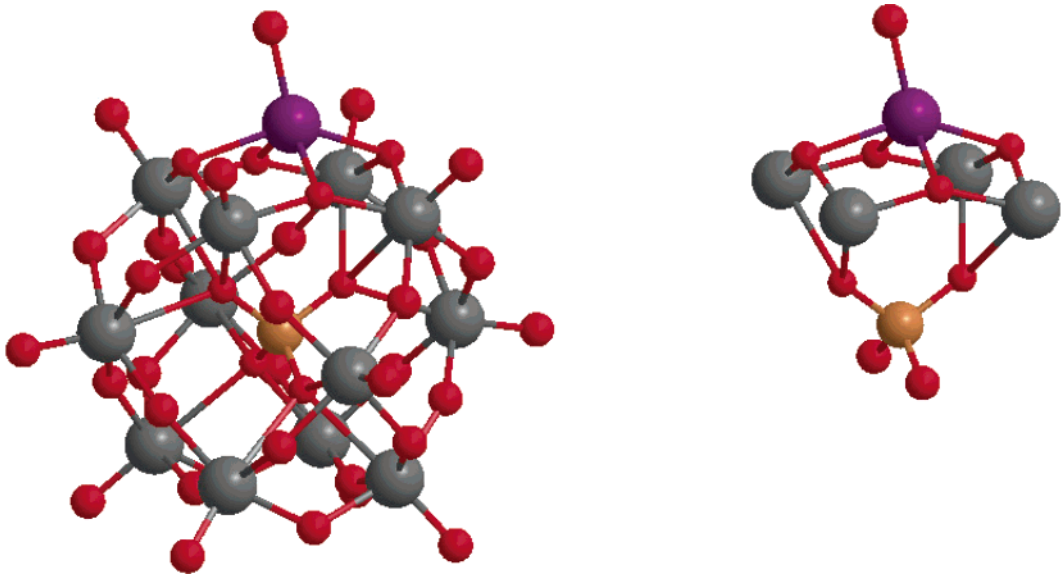

Figure 6. Structure of the vanadyl complexes in fresh (as well as thermally treated) $Cs_4PVMo_{11}O_{40}$ deduced from the ENDOR investigations: VO^{2+} coordination to four oxygen atoms O(2) and O(3) and the V═O bond direction pointing away from the heteropoly anion, forming an angle of 12° with the vector joining V and P. For clarity, the whole Keggin anion (left) including the VO^{2+} unit (top, V = dark ball) and a slice of the relevant section $PO_4Mo_4O_4VO$ of identical orientation (right) is given (in contrast to reality, metal ion radii larger than O^{2-} radii were used).

square-pyramidal geometry. A schematic drawing of the complex structure is shown in Figure 6. The pyramid is formed by the coordination of two O(2) and two O(3) atoms to the vanadyl. At the apex of the pyramid, the vanadyl oxygen is located away from the Keggin anion, and the V═O bond forms an angle of 12° with the vector joining the central P and the V atom. Due to the tilt of the vanadyl bond direction with respect to the V−P direction, a slight shift of the vanadyl ion from the center of gravity of the four oxygens is reasonable. The V−P distance of $r_{V-P} = 3.96$ Å and the crystallographic positions of the O(2) and O(3) oxygen positions were determined for both O(2) oxygens as well as for one of the O(3) oxygens to be $r_{V-O} = 1.9$ Å and for the other O(3) oxygen to be $r_{V-O(3)} = 2.4$ Å. The obtained angle of $\beta = 12°$ agrees with the experimental findings. Although the proposed coordination geometry seems to be very likely, our experimental findings cannot strictly exclude the formation of a trigonal-pyramidal structure with the coordination of three O(2) atoms. Structures similar to the VO^{2+} complexes were proposed for the dehydrated pure HPA materials.[8]

Because an almost exact concordance of the ^{31}P Mims ENDOR spectra of PVMoCs-1 and PVMoCs-2 at selected orientations was obtained (Figure 5), the determined structural model for the VO^{2+} complexes in fresh $Cs_4PVMo_{11}O_{40}$ materials is also formed in the thermally treated sample. In contrast to earlier results using pure HPA materials,[8] in which two entirely different structures were found before and after thermal treatment, heating to 573 K does not influence the coordination geometry of vanadyl complexes in $Cs_4PVMo_{11}O_{40}$ heteropoly compounds.

Obviously, only V^{5+} ions can be incorporated into the molybdenum sites of the Keggin anion $PVMo_{11}O_{40}^{3-}$. This seems reasonable due to charge compensation (V^{4+} has two positive charges less than Mo^{6+}!). The reduction of V^{5+} to V^{4+} is only possible for (a few) "surface"-bound (outer oxygen ions) vanadium ions in the Keggin unit. The reduction of V^{5+} located on Mo^{6+} sites within the Keggin anion would be accompanied by vanadium migration to the Keggin surface and thus by a distortion and/or destruction of the Keggin structure. This is pronounced during thermal treatment of the pure acid $H_4PVMo_{11}O_{40}$, but clearly less distinct for the Cs_4 salt due to the structural rigidity and the spatial demand of the Cs ions and due to the lack of water. The slight differences in the structure of VO^{2+} in the acid and the Cs salt can be explained in the same manner. For a more detailed understanding, information about $V^{IV}-V^{V}$ and $V^{IV}-Cs$ interactions is of particular importance. Corresponding investigations by ENDOR (V^{4+} as probe) and ^{51}V-solid-state NMR spectroscopy are in progress.

6. Conclusions

The better orientation-selectivity of pulsed ENDOR experiments at Q-band frequencies as compared to the conventional X-band approach offered the opportunity to study the location of paramagnetic V(IV) (VO^{2+}) species in fresh and thermally treated $Cs_4PVMo_{11}O_{40}$ heteropoly compounds. In these materials, the heteropolyanions have the well-known structure of the Keggin ion. Using orientation-selective phosphorus ENDOR measurements, the ^{31}P superhyperfine coupling tensor was determined. The VO^{2+} ions were found to be attached to the outer surface of the heteropolyanion, probably coordinated to four outer oxygens, O(2) and O(3), and forming a distorted square-pyramidal complex geometry. The distance between the central phosphorus atom and the paramagnetic vanadium is 3.96 Å. The angle between the V═O bond direction and the vector joining the P and V atom is 12°. With these results, it can be excluded that the vanadyl ions are located at molybdenum sites within the Keggin molecule and that they move to bridge-type positions between the Keggin units. These findings apply for both the fresh and the thermally treated $Cs_4PVMo_{11}O_{40}$ materials. Thermal treatment up to 573 K does not influence the complex structure of the paramagnetic vanadyl species in the cesium (Cs_4) salt of $PVMo_{11}O_{40}$.

Acknowledgment. This research was supported by the Deutsche Forschungsgemeinschaft (Grants PO 426/3-1 and KO 1458/8-1) and the Fonds der Chemischen Industrie.

JA030576Z